Yb3+ ions distribution in YAG nano-ceramics analyzed by both optical and TEM-EDX techniques

ARTICLE *in* THE JOURNAL OF PHYSICAL CHEMISTRY C · JUNE 2014

Impact Factor: 4.77 · DOI: 10.1021/jp502882j

THE JOURNAL OF PHYSICAL CHEMISTRY C

Article

pubs.acs.org/JPCC

Yb^{3+} Ions Distribution in YAG Nanoceramics Analyzed by Both Optical and TEM-EDX Techniques

Georges Boulon,[†,*] Yannick Guyot,[†] Malgorzata Guzik,[‡] Thierry Epicier,[§] Pawel Gluchowski,[∥] Dariusz Hreniak,[∥] and Wieslaw Strek[∥]

[†]Institute Light Matter (ILM), UMR 5306 UCB Lyon 1-CNRS, University of Lyon, Bât. Kastler, 69622 Villeurbanne, France

[‡]Faculty of Chemistry, University of Wroclaw, 14 F. Joliot-Curie, PL-50-383 Wroclaw, Poland

[§]MATEIS, UMR 5510 CNRS, INSA of Lyon, University of Lyon, Bât. B. Pascal, 69621, Villeurbanne, France

[∥]Institute of Low Temperature and Structure Research, Polish Academy of Sciences, ul. Okolna 2, PL-50-422 Wroclaw, Poland

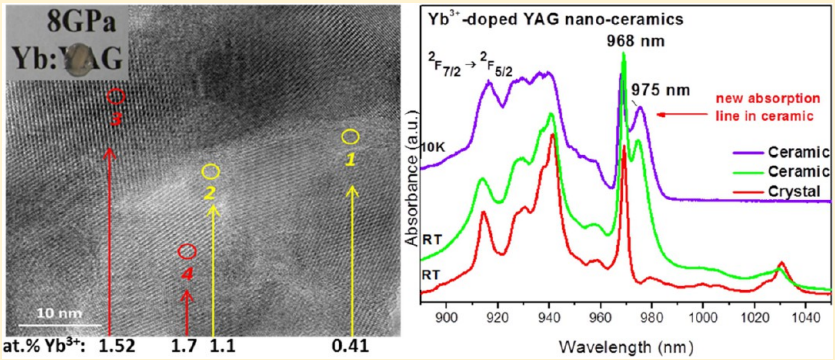

ABSTRACT: We show the approach in the structural and spectroscopic analysis of Yb^{3+}-doped YAG nanoceramics prepared using the low temperature-high pressure sintering technique (LTHP) by conjugation of both TEM-EDX and optical techniques. Pressure sintering dependences of absorption, emission, and decays are analyzed and interpreted. The sample pressurized at 8 GPa for sintering is characterized by the highest transparency and confirms the $Y_3Al_5O_{12}$ garnet structure of the grains of ~21 nm average size. Yb^{3+} ion distribution has been analyzed by both TEM-EDX evaluation in grains and grain boundaries and spectroscopy of Yb^{3+} pairs of small population from the co-operative luminescence phenomenon. EDX analysis at the TEM scale provides unambiguous results on a clear tendency of almost uniform Yb^{3+} distribution. An important new observation has been made at 4 K and room temperature with the $^2F_{7/2} \rightarrow {}^2F_{5/2}$ 0-phonon absorption line located at 975.7 nm, in addition of the 0-phonon line of the YAG structure of grains at 968 nm similar to that of bulky YAG single crystals. We have discussed the origin of this new 0-phonon line relaxing only by nonradiative transitions and conclude that this line might be assigned to Yb^{3+} distorted sites on the grain surfaces.

INTRODUCTION

Yttrium aluminum garnet $Y_3Al_5O_{12}$ (YAG) is a very well-known compound since 1964, widely applied as a matrix for lanthanide based phosphors.[1−3] Great interest in this compound is a result of its special properties such as high chemical stability (melting point at 1940 °C), high thermal conductivity (14 W m^{-1} K^{-1}), isotropic cubic structure, and large energy gap (6.5 eV), so that this material is a good electric insulator. YAG is an active laser crystal in the near-infrared with such rare earth dopants as Nd^{3+}, Ho^{3+}, Er^{3+}, Tm^{3+}, and Yb^{3+} and it is even used for a window material substituting for sapphire. However, there are some limitations in the growing of rare earth-doped YAG crystals, especially by the Czochralski technique merged with the increasing of the concentrations of dopants, with the fabrication of potential shapes and finally with the cost. The need of prospect other types of materials lead to transparent polycrystalline ceramics of cubic structure as a new generation of optical materials. Huge efforts were necessary to successfully fabricate high quality rare earth-doped $Y_3Al_5O_{12}$ laser ceramics. Before 1995, it was considered that ceramic materials cannot be used for lasers, because the optical quality of conventional ceramics was quite low. Laser ceramics require indeed no optical scattering and perfect homogeneity and finally Nd^{3+}-doped YAG laser ceramic emerged from pioneering works of Ikesue (World Lab. Co., Ltd., Nagoya)[4,5] and advanced researches.[6,7] Another Japanese group (Yagi's group) from Konoshima Co. has succeeded to get nice advances with laser ceramics.[8−11] Nowadays laser ceramics are commercially available. The already described YAG ceramics have a grain size in the range of a few micrometers.

There is also interest in synthesis and optical properties of rare earth-doped YAG nanocrystalline ceramics.[12,13] YAG

Received: March 23, 2014
Revised: June 17, 2014

   dx.doi.org/10.1021/jp502882j | J. Phys. Chem. C XXXX, XXX, XXX−XXX

nanopowders may be synthesized by several methods including sol−gel,[14] Pechini,[15] solvothermal,[16] combustion,[17] and coprecipitation.[18] For preparation of high optical quality ceramics both structurally pure and nonaggregated nanopowders are required. However, less work has been done to sinter nanocrystalline ceramics.[19−31] Dense ceramics with nanograin size may display new structural, magnetic, electric, or electronic properties with great potential for applications. However, sintering usually causes grain growth in the micrometer range. There are three main methods to prevent grain growth during sintering:[19] application of hot-pressing or sintering forging, addition of dopant to modify diffusion process, and sintering powders in metastable crystallographic phases that during sintering act as seeds for the final phases. The third one is used for such materials like TiO_2 and Al_2O_3.[20,21] For example nanoscale glass-ceramic alumina doped by rare earth oxides (Nd_2O_3, Eu_2O_3, and Er_2O_3) with transparency in the mid-infrared range can be achieved by heating for a short time bulk glasses.[22] Also nonconventional sintering methods like microwave sintering,[23,24] shock or dynamic consolidation,[25,26] field assisted sintering,[27,28] and high pressure low temperature sintering[29−31] are applied.

Naturally, the first nanoceramics developed were Nd:YAG nanoceramics.[12,13] They were obtained by using the high pressure low temperature (HPLT) technique.

This method allows the synthesis of transparent YAG nanoceramics composed of the nanometric grains comparable with the sizes of starting nanopowders. These materials are potentially attractive for many applications since reduction of the grain size to the nanometer scale can improve their physical and mechanical properties. In particular the effect of applied pressure on preparation of transparent YAG nanoceramics was studied.

The optimal sintering conditions for obtaining optically transparent nanoceramics are temperature of 450 °C and pressure of 8 GPa. As result, a nanoporous and transparent sample with 37 nm grains was obtained with the extinction coefficient equal to 13.6 cm^{-1} at 1064 nm. Uniform distribution of nanosized pores in the ceramics has been observed, which contributes to scattering of transmitted light.

We have continued this research by selecting Yb^{3+} ion used either as sensitizer for other rare earth ions or for direct laser ion or still as a structural probe ion. The state-of-art of Yb^{3+}-doped inorganic materials in both basic and applied research was developed in the following articles.[32,33] Especially for YAG host we made a detailed structural and spectroscopic analysis of Yb^{3+}-doped YAG of bulky shape,[34] nanocrystallite shape,[35] transparent ceramic shape[36,37] and also transparent nanoceramic shape[38] allowing comparison of these type of materials.

Recently, white anti-Stokes emission was observed in Yb:YAG nanocrystalline ceramics and investigated under focused beam of 976 nm laser diode (LD) excitation.[39] The emission intensity increased significantly with concentration of active ions. This effect was more pronounced in vacuum compared to atmospheric pressure. Only for full concentrated YbAG nanoceramic white emission could be observed in normal atmosphere pressure. These new phenomena should be understood and we think we should first investigate both structural and spectroscopic analysis of these nanoceramic samples fabricated from the nanocrystalline powders, by combining X-ray, TEM-EDX, absorption, emission and decay measurements. In particular, new important results on the effect of applied pressure during sintering process on the absorption spectra at low temperature (4 K) and emission spectra will be investigated. In addition, Yb^{3+} ion distribution in nanoceramics will be also analyzed by both spectroscopy of Yb^{3+} pairs from the cooperative luminescence spectra and TEM-EDX evaluation of Yb^{3+} concentrations in grains and grain boundaries.

EXPERIMENTAL SECTION

Synthesis of Transparent Nanoceramics. All the samples investigated in this work were prepared in the Institute of Low Temperature and Structure Research of Polish Academy of Sciences in Wroclaw. The initial YAG nanopowders doped with a nominal ytterbium ions molar concentration between 0.5% and 100% vs yttrium ions were prepared using modified Pechini method described elsewhere.[15] Nanoceramics composed of nanosized grains were fabricated by the low temperature-high pressure sintering technique (LTHP).[13] Before sintering, pellets of diameter 5 mm and height about 2.5 mm were formed from the nanopowders (obtained at 900 °C) by cold pressing under pressure of 50 MPa. The pellet was placed in the container in graphite tube used as a resistance heater. Green body was separated from graphite by boron nitride (BN). The force exerted by the anvils creates a quasi-isostatic pressure between 2 and 8 GPa. The samples were sintered at temperature 450 °C during 1 min. The scheme of the equipment used for fabrication of the samples is presented in Figure 1.

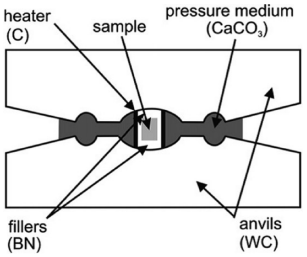

Figure 1. Scheme of the cell used in this work:[13] pressure 2−8 GPa, temperature 450 °C, time 1 min, YAG nanopowder obtained at 900 °C.

Figure 2 shows the photos of the ceramics obtained under different pressures, i.e., green body (without any pressure) and

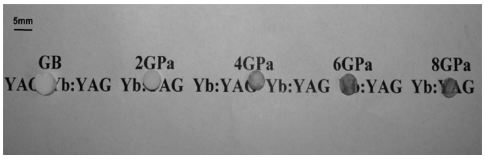

Figure 2. Photos of green body (GB) and nanoceramics samples under 2, 4, 6, and 8 GPa pressures, respectively.

2, 4, 6, and 8 GPa, respectively. As one can see the transparency is changing with the pressure and the best is observed for the samples 6 and 8 GPa.

X-ray Powder Diffraction (XRD). Data have been obtained at the "Diffractométry Center Henri Longchambon" of the University Lyon1 and the Laboratory of X-ray Crystal Structure Analysis at the Faculty of Chemistry, University of Wroclaw. The powdered crystal diffractograms were recorded by using a Bruker D8 ADVANCE powder diffractometer with

dx.doi.org/10.1021/jp502882j | J. Phys. Chem. C XXXX, XXX, XXX−XXX

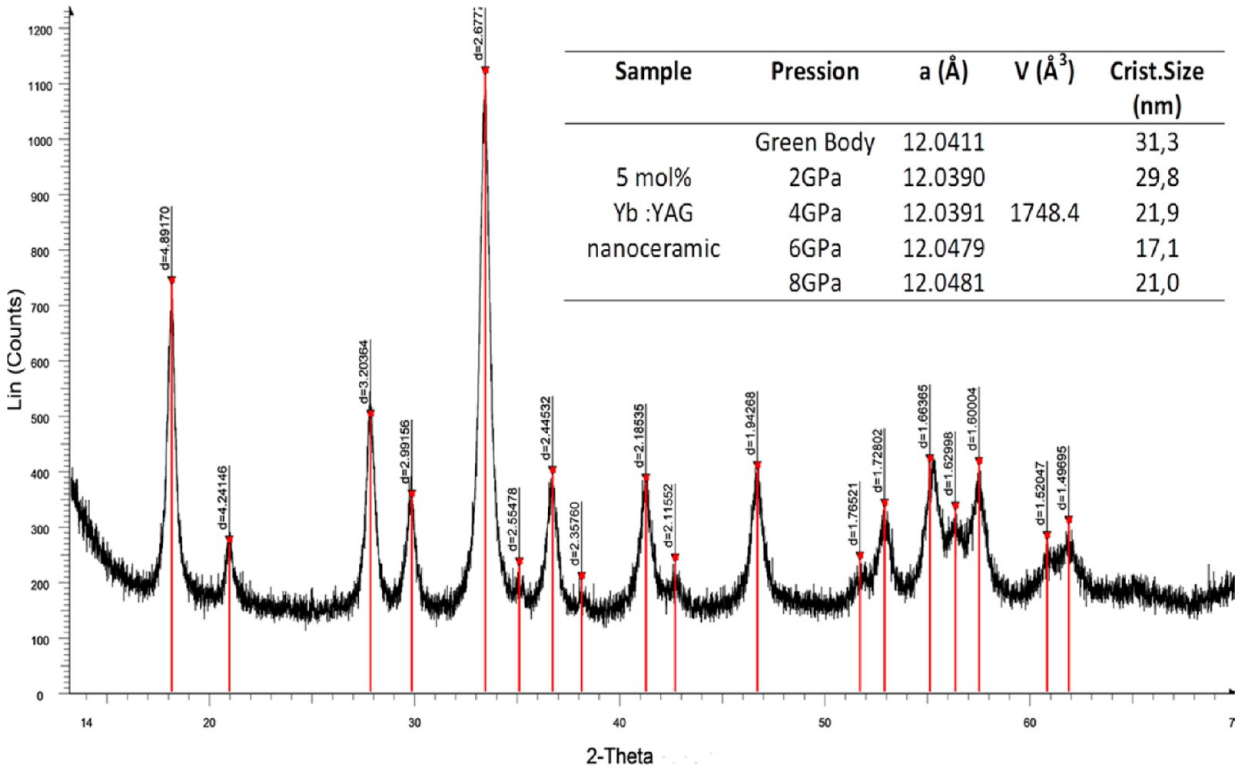

Sample	Pression	a (Å)	V (Å^3)	Crist.Size (nm)
	Green Body	12.0411		31,3
5 mol%	2GPa	12.0390		29,8
Yb :YAG	4GPa	12.0391	1748.4	21,9
nanoceramic	6GPa	12.0479		17,1
	8GPa	12.0481		21,0

Figure 3. XRD pattern of 5 mol % Yb^{3+}-doped YAG nanoceramic sintered at 450 °C. Insert: Pressure dependence of the cell parameter and the average grain sizes.

nickel-filtered Cu Kα radiation (λ = 1.5418 Å) and a Vantec detector. The measurements were performed within 2θ range of 10−70° with the scan rate 0.008° per step and the counting time 4 s per step.

Transmission Electron Microscopy (TEM). TEM experiments were conducted on thin foils classically prepared by ion beam thinning (PIPS Gatan), using a JEOL2010F field emission gun transmission electron microscope operating at 200 kV. The microscope was fitted with an Oxford EDX (energy dispersive X-ray) analyzer for elemental chemical analysis at MATEIS-INSA of Lyon. Detector of the latest generation was used, a SDD (Silicon Drift Detector) X-MAX 80 from Oxford Instruments. This technology provides a much better counting rate and sensibility limit than conventional detectors based on a Si−Li diode. The setup is the same as that used in our recent paper on the spatial distribution of the Yb^{3+} rare earth ions in $Y_3Al_5O_{12}$ and Y_2O_3 optical ceramics as analyzed by TEM.[40,41] This offers a great advantage in the present context of measuring small quantities (and their possible small variations) of rare earth elements in optical ceramics. Since one of the major goals of this work is to study the homogeneity of the dopant distribution near and at grain-boundaries, most EDX measurements reported in the following were performed with a nanoprobe, the size of which will be given through the value of its full-width at half-maximum (fwhm, in nm). The quality of high resolution TEM images recorded on most analyzed grain-boundary areas indicates that the thickness is not nominally greater than 20 nm; this gives a beam broadening of the order of 2.4 nm in YAG. These numeric values indicate that with an incident nanometric probe, the spatial resolution of EDX analysis remains reasonably good. As usual in EDX-TEM, all results will be given in atomic % (at. %), with the total composition included all atomic species (O, Y, Al and the doping rare earth element) normalized to 100%.

Spectroscopic Measurements. *Absorption Spectra.* Absorption spectra in the 800−1150 nm spectral range were recorded at 4 and 293 K with a Cary-Varian 5000 Scan spectrometer equipped with an Oxford CF 1204 helium flow cryostat at the Chemistry Department of the University of Wroclaw.

Emission Spectra. Emission spectra and decays of fluorescence were recorded at the Institute Light Matter (ILM) of the University of Lyon. Nd:YAG impulse laser equipped with Ti:sapphire oscillator was used as excitation sources for the emission spectra and decays measurements. The emission spectra were measured with a Jobin−Yvon THR 1000 monochromator and Synapse Horiba Jobin Yvon CCD camera. Emission decays were recorded with a LeCroy WaveSurfer 400 oscilloscope. All spectra were corrected for the sensitivity and wavelength of the experimental setup.

RESULTS AND DISCUSSION

Structural Characterization from XRD Pattern. Previous characterizations of semitransparent nanocrystalline YAG ceramics doped with 1 mol % Nd^{3+} and 5 mol % Yb^{3+} have been done by the research group from the Polish Academy of Sciences.[13] The grain size of the sintered pellets was in the range of 25 nm. It was observed that during high pressure sintering YAG decomposes into YAP and alumina. The decomposition of the YAG particles and transformation to the much larger YAP crystals was confirmed by the coexistence of the broad peaks originating from YAG (JCPDS No. 33−40) and the sharp reflexes from YAP structure (JCPDS No. 16−219), which is observed for samples pressed at 550 °C, 600 °C

dx.doi.org/10.1021/jp502882j | J. Phys. Chem. C XXXX, XXX, XXX−XXX

and also at higher temperatures. The decomposition process started even at 550 °C according to the reaction:

$$Y_3Al_5O_{12}(YAG) \rightarrow 3YAlO_3(YAP) + Al_2O_3 \quad (1)$$

as deducted from on line X-ray diffraction as a function of temperature and pressure.

On the basis of these results, to avoid decomposition, all samples analyzed in this paper were sintered at 450 °C.

Figure 3 confirms the garnet structure of the 5 mol % Yb^{3+}-doped $Y_3Al_5O_{12}$ nanoceramics and the inset shows the evolution of the structural data of the cell parameter (in Å), and the average grain sizes (in nm), calculated from the usual Scherrer equation.

If pressure is increasing from green body to 8 GPa, the cell parameter is increasing, whereas the grain size is decreasing but seems to increase again between 6 and 8 GPa (see insert in Figure 3). Comparison of the refined values of the lattice parameters for pure $Y_3Al_5O_{12}$ (a = 12.009 Å) shows the increase of the lattice parameters for Yb^{3+}-doped YAG, which proves a partial substitution of ytterbium ions (ionic radii of 86.8 pm by Shannon and Prewitt) for yttrium (ionic radii of 90 pm) sites in the garnet lattice like for Nd^{3+}-doped YAG.[42] Confrontation of the resulting diffraction patterns with the reference standard of the YAG confirms the presence of only one $Y_3Al_5O_{12}$ garnet cubic crystalline phase. We did not detect any new amorphous phase probably due to the small concentration of this phase.

Characterization of the Yb^{3+} Ions Spatial Distribution by TEM-EDX Technique. *Analytical Results from EDX on a Large Area.* We have selected the sample pressurized at 8 GPa which has been characterized by the highest transparency (see Figure 2). The same procedure was applied in Yb^{3+}-doped nanoceramics samples like for the Yb^{3+}-doped YAG[36,37] and the Ce^{3+}-doped YAG bulky ceramics.[40,41] The sample was first polished to a thickness of about 100 μm and then mechanically grinded to produce smaller debris. These thinner parts were then sandwiched between initial larger pieces and crushed into a quartz mortar (such sandwich procedure prevents from any undesirable contamination from the mortar). The resulting agglomerates were then deposited on a classical holey carbon grid.

We have measured different areas of both grain boundaries and grains of these nanoceramics. TEM photographs of grains and grain boundaries are shown in Figure 4. Table 1 summarizes the analytical results from EDX (on a large area) in atomic %.

The chemistry of the material is consistent with the YAG composition, apart from the detection of a systematic small content of silicon by SiO_2 silica, a slight excess in aluminum by Al_2O_3 and a smaller Yb^{3+} content than expected (1.7 at. % instead of 3 at. % for over more than 20 analysis points inside grains and at grain boundaries).

The nanostructure consists of small crystallites in the range 5−20 nm (rough estimate). At grain "triple junctions" which is quite difficult to define with sub nanograins, an amorphous-type contrast is frequently revealed in high resolution micrographs (see the arrow in Figure 5) but its concentration was not high enough to determine the real composition.

The most striking feature of the EDX results in these samples is the absence of Yb^{3+} ions segregation in grain boundaries like it was observed in bulky YAG garnet and Y_2O_3 sesquioxides.[36,37] Yb^{3+} cations were not seen as being concentrated in perfect grain boundaries in Figure 6, contrary to Ce^{3+}

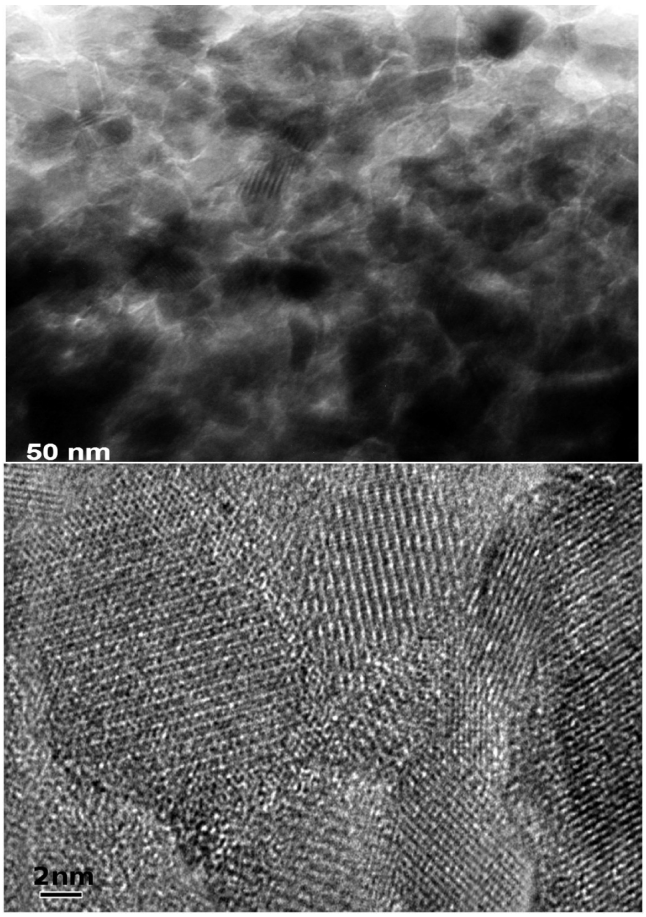

Figure 4. TEM images of the 1.7 at. % Yb^{3+}-doped YAG nanoceramics fabricated at 450 °C under 8 GPa.

Table 1. Contents (in at. %) of O, Al, Si, Y, and Yb Elements on Large Area Presented in Figure 4

elements	at. % O	at. % Al	at. % Si	at. % Y	at. % Yb	at. % Y +Yb
Expected Yb^{3+}-doped YAG	60%	25%	0%	12%	3%	15%
From spectra	at. % O	at. % Al	at. % Si	at. % Y	at. % Yb	at. % Y +Yb
Global analysis	60.0%	25.6%	0.4%	12.3%	1.7%	14.0%

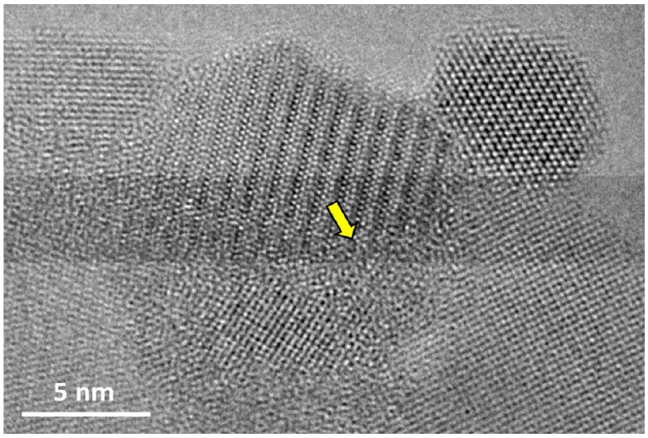

Figure 5. Nanostructure of Yb^{3+}-doped YAG nanoceramics as observed by high resolution imaging technique (HREM).

dx.doi.org/10.1021/jp502882j | J. Phys. Chem. C XXXX, XXX, XXX−XXX

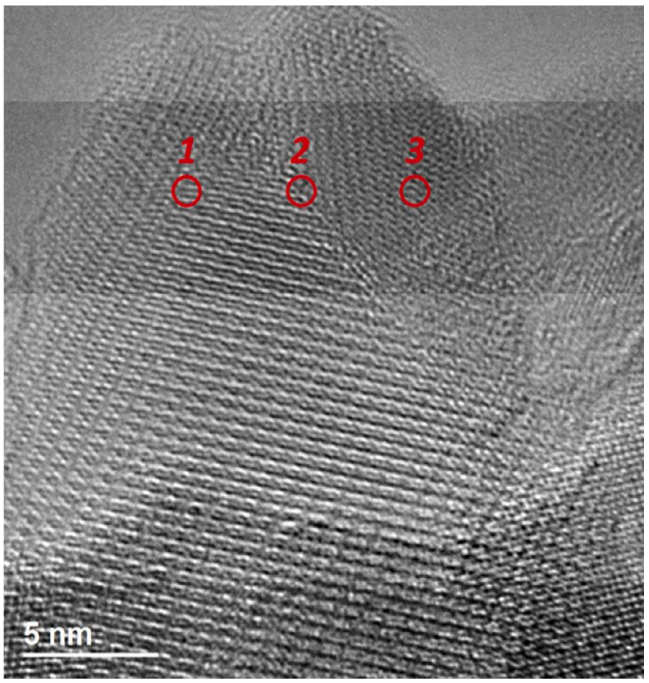

Figure 6. TEM images of 3 different positions in Yb^{3+}-doped YAG nanoceramics areas: crystalline grains (1 and 3) and perfect grain-boundaries (2).

cations[40,41] or Nd^{3+} cations.[43] For this spatial area of observation, values of 2.1 and 2.5 at. % have been reported in Table 2, higher than the average value of 1.7 at.%.

Table 2. Concentrations of the Main Atoms in Three Positions of the Horizontal Line Acrossing the Grain Boundary in Yb-Doped YAG Nanoceramics As Shown in Figure 6

spectrum	% at. O	% at. Al	% at. Si	% at. Y	% at. Yb	Y+Yb
position 1	60.0	23.0	0.5	14.4	2.1	16.5
position 2	60.0	25.7	0.0	12.3	2.1	14.4
position 3	60.1	22.0	1.6	13.8	2.5	16.3

Another TEM-EDX measurement have been performed in 4 different positions shown in Figure 7 within crystalline grains and grain boundaries where an amorphous phase is clearly seen in a small area. The Yb concentrations are reported in Table 3. It can be seen two values of 1.52 and 1.7 at. % for crystalline grains as expected earlier but much less, 0.41 and 1.1 at. %, in the position of the amorphous grain boundaries.

These results clearly show that there is a little variation in the Yb^{3+} content at the grain-boundary and within the adjacent grains, especially when the grain boundaries contain an amorphous phase and does not exist when the crystalline grains are perfectly joined. For comparison, differences of a factor of 4 were detected for the Ce^{3+} concentration in Ce^{3+}-doped YAG ceramics, 4 times higher inside the grain boundary than inside the crystalline grains. Due to the near-infrared emission of Yb^{3+} rare earth ions, it was not possible to observe such segregation by using the confocal microscopy technique as it was used with Ce^{3+} ions emitting an intense luminescence band in blue, green and yellow ranges easy to detect with photomultipliers.[40,41] However, EDX analysis at the TEM scale provides unambiguous results and we can conclude here a clear

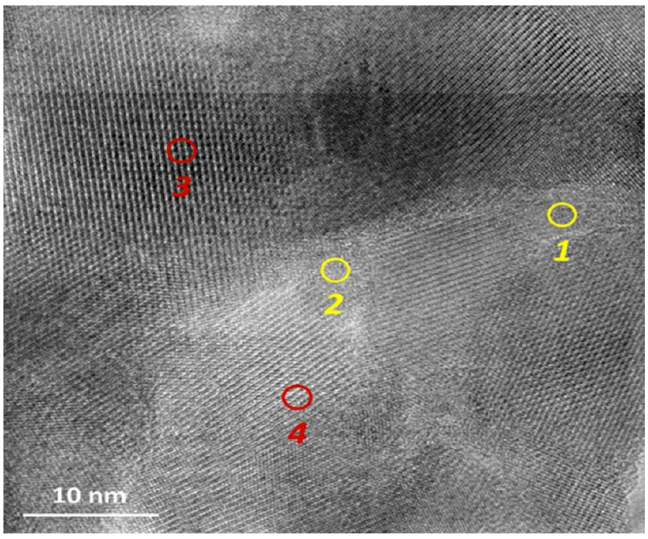

Figure 7. TEM images of 4 different positions in Yb^{3+}-doped YAG nanoceramics in which we observe an amorphous phase in the grain-boundaries (1 and 2). Crystalline grains are analyzed in Table 3

Table 3. TEM Evaluations of Four Different Positions in Yb^{3+}-Doped YAG Nanoceramics Areas in Figure 7[a]

elements	O	Al	Si	Y	Yb
expected contents in at. %	60	25	0	12	3
position 1	60.21	28.7	0.94	9.73	0.41
position 2	60.03	28.97	1.13	8.78	1.1
position 3	60.08	23.45	0.6	14.35	1.52
position 4	60.02	19.38	0.6	17.96	1.7

[a]Amorphous phase of grain-boundaries: 1 and 2. Crystalline grains:3 and 4. All the concentrations are evaluated in at. %.

tendency of rather uniformity of Yb^{3+} distribution between grains and grain boundaries of perfect nanoceramics in the similar way of bulky ceramics.

All the previous experimental results correlate well with low segregation coefficients of Ce^{3+} and Nd^{3+} large rare earth cations, but higher segregation coefficients for small rare earth cations like Yb^{3+} in the garnet structure observed in the melt crystal growth and thin film liquid phase epitaxy from flux.[44−48] The data on segregation in melt/flux crystal growth are widely available and can be used for preliminary estimation of the dopant distribution in solid-state ceramic processing. The lower is the segregation coefficient of dopant in the melt growth, the greater is amount of dopant collected on the grain boundaries of the ceramic polycrystalline materials. This could help to predict the highest uniformity of Yb^{3+} dopant distribution. The large difference of values of the segregation coefficients (0.08 for Ce^{3+}, 0.18 for Nd^{3+} and 1.09 for Yb^{3+} respectively) in YAG ceramics[49] explains also the respective behavior of the distribution of these luminescent cations inside the volume of nanoceramics with especially a high segregation for Ce^{3+} and Nd^{3+} and much more regular distribution for Yb^{3+} ions.

Although fluctuations occur, no evidence is clearly found for any Yb^{3+} segregation of next neighbor's ions at interfaces of grains. Yb^{3+} contents exhibit similar scattering inside the 2 nm value of the probe beam. Then the main conclusion from TEM-EDX measurements is related to the absence of Yb^{3+} aggregates either in grains or in grain boundaries of the examined areas which excludes the concept of the main energy lost by

dx.doi.org/10.1021/jp502882j | J. Phys. Chem. C XXXX, XXX, XXX−XXX

nonradiative transitions during resonant migration of the 0-phonon line $^2F_{7/2}$ (1) ← →$^2F_{5/2}$ (5) at 975 nm as it will be analyzed later on.

Optical Spectroscopic Properties of Yb^{3+}-Doped YAG Nanoceramics. *Energy Level Diagram.* First, let us remind the energy level diagram for $^4f_{13}$ configuration of Yb^{3+} ions as shown in Figure 8.[32] This is the simplest diagram of the rare

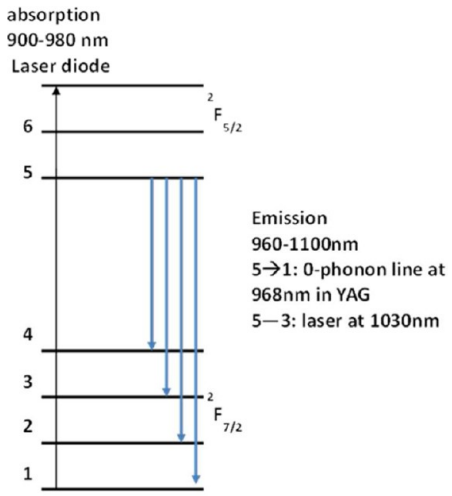

Figure 8. Yb^{3+} energy level diagram for the $^4f^{13}$ configuration in the near IR range.[32] Characteristics: pumping by powerful laser diodes at 940 nm (1 → 6) or 980 nm (1 → 5); due to Boltzmann population of the stark levels of the $^2F_{7/2}$ manifold, this is a quasi-4 level laser scheme; the total spin quantum number is half integer and in the crystalline field the maximum number of levels is $(2J + 1)/2$ (Kramers' degeneracy); small quantum defect between absorption and emission leads to a low thermal loading; usually laser output at around 1030 nm by 5 → 3 and tunable laser by 5 → 2, 3, 4.

earth ions. All transitions are located in the near-infrared spectral region: 1 → 5, 6, 7 absorption lines between 900 and 1000 nm and 5, 6, 7 → 1, 2, 3, 4 emission lines between 940 and 1100 nm. The resonance lines 1 → 5 and 5 → 1 so-called 0-phonon lines in both absorption and emission spectra are the usual structural probes to assign all transitions in materials, with intensities depending of the radiative energy transfer inside the volume of the materials.

Absorption Spectra and the Observation of a New Line Only in Nanoceramics. The main feature to be noticed is the first observation in all nanoceramics of the double 0-phonon absorption line transition $^2F_{7/2}$ (1) → $^2F_{5/2}$ (5) around 968.3 and 975.9 nm, respectively at RT and 968 and 975 nm, respectively at 10K, as an example in 5 mol % Yb^{3+}-doped YAG nanoceramics (Figures 9−12). The highest energy line at around 968.3 nm is characteristic of Yb^{3+} ions in the YAG garnet structure. The lowest energy line is only specific of nanoceramic samples, not observed in single crystals as clearly seen in Figure 10. We have especially analyzed the sintering pressure dependence of the absorption spectra at RT (Figures 10-11) and also at 4 K (Figure 12). Two important observations have to be mentioned: the bandwidth is much higher than that of the garnet structure and the intensity of this new absorption line at RT is increasing with the sintering pressure between 4 and 8 GPa. The characterizations of these lines have been done in Figure 12.

This is important to justify why the sample pressurized under 8 GPa as seen in Figure 2 has been choose in the 2.3 section.

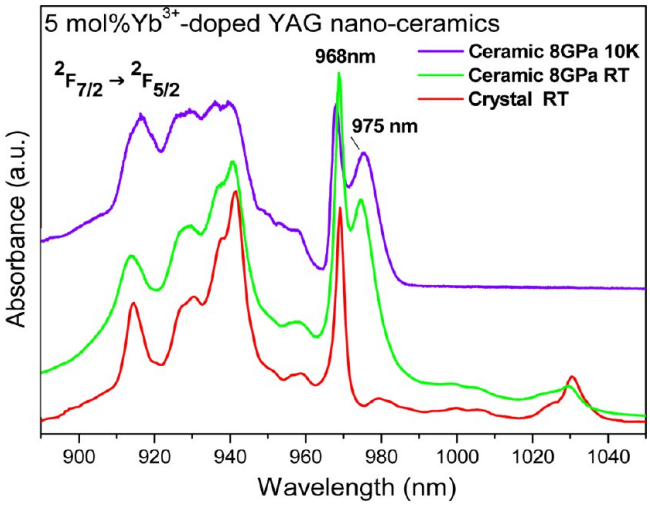

Figure 9. Comparison of the absorption spectra in 5 mol % Yb^{3+}-doped YAG nanoceramics at RT and 10 K and Yb^{3+}-doped YAG crystal at RT.

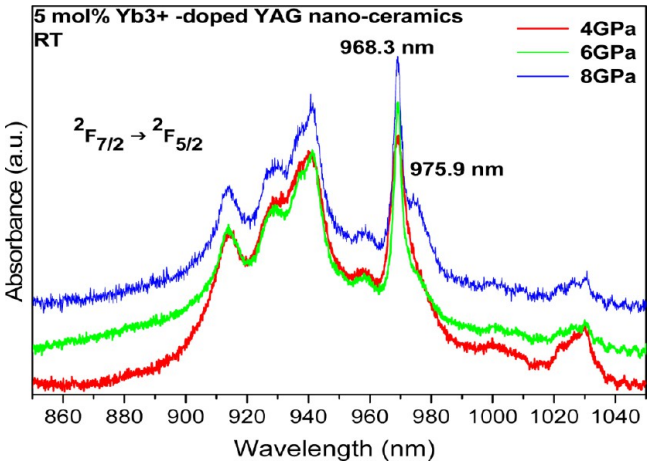

Figure 10. Pressure dependence of the absorption spectra in 5 mol % Yb^{3+}-doped YAG nanoceramics under 4, 6, and 8 GPa respectively at RT.

The transmission spectra in Figure 13 shows clearly an increasing of the transmittance from 4 to 8 GPa from UV to near IR regions. The most probable reason is higher pressures reduce porosity of nanoceramics samples prepared by high pressure low temperature sintering as it has been already shown in Nd^{3+}-doped YAG nanoceramics.[13]

It means this new 0-phonon line might be connected especially with strains associated with the application of the pressure.

If the 0-phonon line at 968 nm can be undoubtedly assigned to regular Yb^{3+} ions in the grain of the YAG garnet structure, at the same energy location that this of bulky YAG single crystals, the question arises about the origin of the new 0-phonon line at the lowest energy.

The first answer can be related with Yb^{3+} distorted sites located in the surface of the nanoceramics, as it is typical for nanomaterials. The pressure dependence recorded for 5 mol % Yb^{3+}-doped nanoceramic in Figure 10 is in favor of the increasing of the population of the sites responsible of this absorption when pressure increases from 4 to 8 GPa.

dx.doi.org/10.1021/jp502882j | J. Phys. Chem. C XXXX, XXX, XXX−XXX

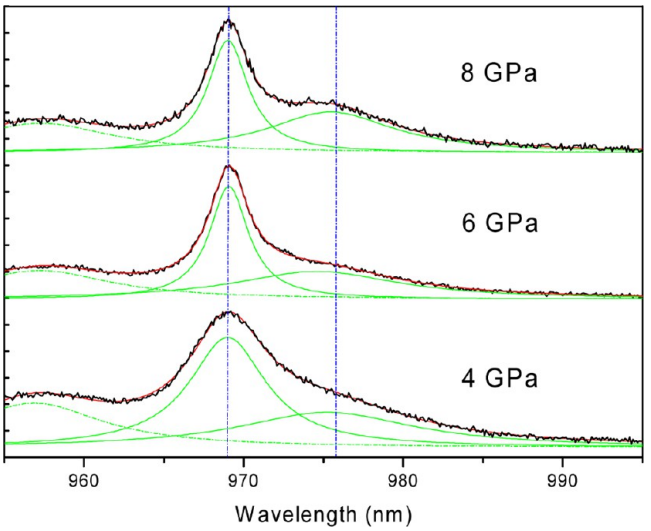

Figure 11. Spectral fits with Lorentz profiles of the $^2F_{7/2}$ (1) → $^2F_{5/2}$ (5) 0-phonon absorption lines near by 968.3 and 975.9 nm respectively and also of the vibronic line near by 957 nm in the 5 mol % Yb^{3+}-doped YAG nanoceramics at RT shown in Figure 10.

Table 4. Main Parameters of the Lorentz Curves Used to Fit Absorption Lines in Figure 11

pressure	area	max in nm	width	height
4 GPa	7.648	969.001	5.872	0.829
	5.595	975.233	13.44	0.265
6 GPa	3.977	969.084	2.982	0.849
	4.111	974.581	12.523	0.209
8 GPa	4.10	969.019	3.088	0.845
	4.667	975.452	9.686	0.307

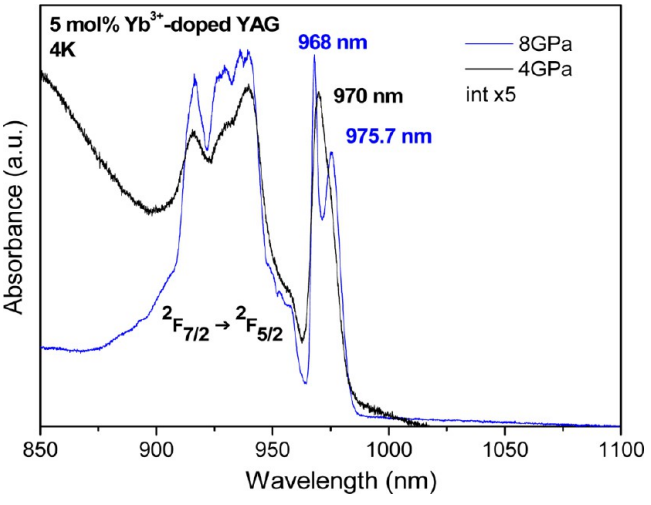

Figure 12. Pressure dependence of the absorption spectra in 5 mol % Yb^{3+}-doped YAG nanoceramics at 4 K.

However, another hypothesis should be considered. This line might be also partially connected to additional traces of crystalline phases, more precisely both Al_2O_3 and $YAlO_3$ phases as a consequence of the decomposition reaction:

$$Y_3Al_5O_{12}(YAG) \rightarrow 3YAlO_3(YAP) + Al_2O_3 \quad (2)$$

This is why we have analyzed absorption spectra of Yb^{3+}-doped $YAlO_3$[50] and Yb^{3+}-doped Al_2O_3.[51,52]

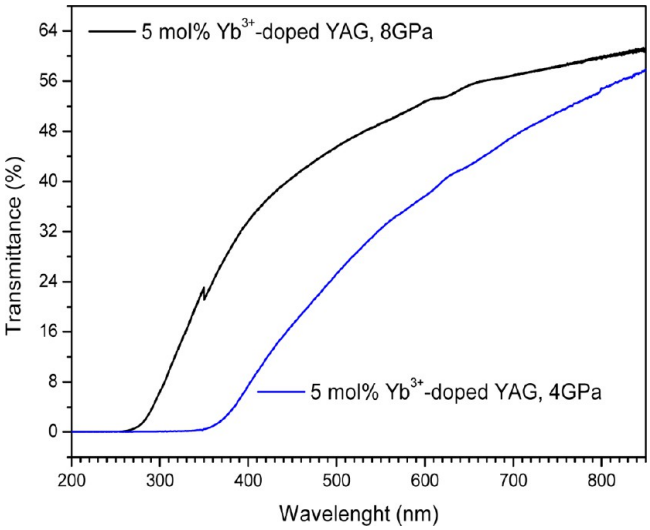

Figure 13. Pressure dependence of the transmission spectra at RT of 5 mol % Yb^{3+}-doped YAG nanoceramics under 4 and 8 GPa, respectively.

The 0-phonon line of $Y_{1-x}Yb_xAlO_3$ is positioned at 978.5 nm at much lower energy than the 975 nm of the Yb^{3+}-doped nanoceramic and so cannot be retained with a detectable amount in these samples as a coherent conclusion of the temperature sintering at 450 °C explained earlier to avoid formation at least of the YAP phase.

As for Yb^{3+}-doped Al_2O_3 thin films[51] or nanopowders,[52] large differences can be seen in spectra of the 0-phonon lines either at 982 nm or at 970 nm. This discrepancy might be due to the presence of the two phases α and θ depending on the temperature.[53]

The best fit is indeed observed with Yb^{3+}-doped α-Al_2O_3 single crystals grown by LHPG technique.[54] It has been noted that only a small amount of Yb^{3+} ions enter the lattice by substitution of Y^{3+} cations and that higher dopant concentration leads to the presence of a variety of Yb^{3+} containing phases like garnet ones. Three Stark components of the $^2F_{5/2}$ manifold are clearly identified in Yb^{3+}-doped α-Al_2O_3 with the highest intensity of the 0-phonon line at 10252 cm^{-1} (975.4 nm). The center frequencies of the lines relative to the ground state are located at 337, 550, and 1020 cm^{-1}. Additional peaks appear for $0.01 < c < 0.05$ at%. $Yb_3Al_5O_{12}$ garnet clusters (10 330 cm^{-1} peak at 968.1 nm) form for $0.1 < c < 0.5$ at%. We can conclude about the possibility to assign this 0-phonon line of Yb^{3+}-doped α-Al_2O_3 single crystals with the new absorption line observed in nanoceramics and also with the possibility to form clusters of $Yb_3Al_5O_{12}$. However, we should insist again on the weak concentration of Yb^{3+}-doped α-Al_2O_3 single crystals which is almost impossible to be detected by XRD and was not detected by TEM so that XRD spectra characterize only YAG phase. If this hypothesis is retained it means there is a coincidence between 0-phonon lines of Yb^{3+} distorted sites of YAG located in the surface of the nanoceramics and that of Yb^{3+}-doped α-Al_2O_3 single crystals but with a much more higher concentration of Yb^{3+} distorted sites in YAG phase.

Another hypothesis can be formulated concerning the presence of traces of SiO_2 silica glass in the samples not from the raw materials but incorporated during polishing operations. In Yb^{3+}-doped silica glasses we have observed this line located at 976 nm in CAS and LSCAS glasses[54] almost in coincidence

dx.doi.org/10.1021/jp502882j | J. Phys. Chem. C XXXX, XXX, XXX−XXX

with that in nanoceramics. Nevertheless, this is difficult to suppose that Yb^{3+} dopants can be introduced in the silicate structure by polishing operations and give high absorption peak equivalent and even stronger than the absorption peak of the regular Yb^{3+} ions in the garnet lattice of grains. Consequently, we do not support this hypothesis.

In conclusion, the new absorption line peaking at 975.7 nm at 4K seems to point out rather Yb^{3+} distorted sites on the grain surfaces of nanoceramics. Probably an additional small amount of Yb^{3+}-doped amorphous unknown phase within some grain boundaries and another additional small amount of Yb^{3+}-doped α-Al_2O_3 single crystals still exists but almost impossible to be detected by XRD and then of negligible influence. In order to get complementary information on this assignment, we will look at the emission spectra and decay times of Yb^{3+} ions in these YAG nanoceramics.

Near IR Emission Spectra. The emission spectra of 5 mol % Yb^{3+}-doped YAG nanoceramic were measured at RT and 77 K and compared with bulky single crystal under pumping with a tunable Ti-sapphire laser in Figures 14 and 15. The

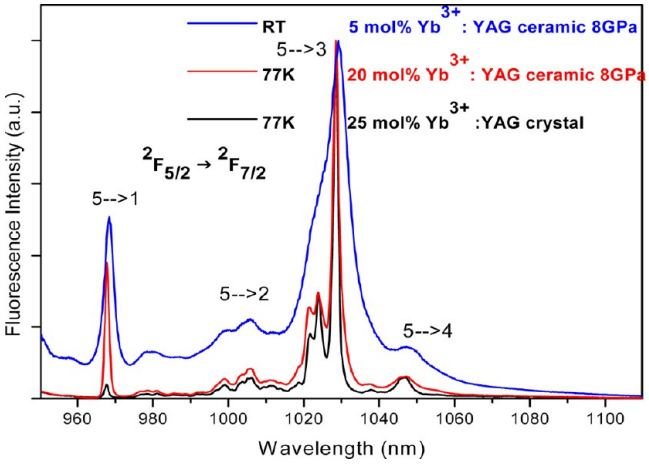

Figure 14. Emission spectra of 5 mol % Yb^{3+}-doped YAG nanoceramics (8 GPa) at RT and 77 K under excitation by 917 nm of a Ti-sapphire laser. The comparison can be done with 25% Yb^{3+}-doped YAG single crystal at 77 K. The 0-phonon lines in emission are 968.4 nm at RT and 967.2 nm at 77 K for the nanoceramics sample and 967.6 nm for the single crystal.

reabsorption phenomenon seen by the intensity of the resonant 0-phonon, line at 967.6 nm of $^2F_{5/2}$ (5) → $^2F_{7/2}$ (1) is very strong in the large volume of the single crystal whereas it does not exist with the 0-phonon line at 967.2 nm in the small volume of the nanoceramic characterized by an average size of 21 nm (see Insert in Figure 3). This reabsorption is associated with the radiative energy transfer, or self-trapping process, by resonance between Yb^{3+} ions, and so can be affected by the nonradiative energy transfer, or self-quenching process, when the effective diffusion average length is high inside the lattice. This lack of reabsorption is confirmed in Figures 15 a) and b) by both pressure and concentration dependences in which we can see always clearly the $^2F_{5/2}$ (5) → $^2F_{7/2}$ (1) 0-phonon lines and even both the $^2F_{5/2}$ (6) → $^2F_{7/2}$ (1) and the $^2F_{5/2}$ (7) → $^2F_{7/2}$ (1) 0-phonon lines inside the nanoscale volume of the samples.

We tried to identify more precisely the two types of centers by pumping selectively two 0-phonon lines with a tunable Ti-Sapphire laser of ~1 cm^{-1} narrow line-width used as pumping source. The results are shown in Figure 16 under the following excitations:

- 917 nm in the $^2F_{5/2}$ (7) highest energy level to display all lines of the emission spectrum,
- 968 nm in the $^2F_{5/2}$ (5) level of the Yb^{3+} ions in the YAG garnet grain,
- 975 nm in the $^2F_{5/2}$ (5) in resonance with this new absorption line assigned previously to Yb^{3+} distorted sites on the grain surfaces of nanoceramics.s

The 917 and 968 nm excitations give rise to the same emission spectra related with $^2F_{5/2}$ (5) → $^2F_{7/2}$ (1, 2, 3, 4) transitions, whereas under 975 nm the radiative probability of the $^2F_{5/2}$ (5) level is almost zero. The very weak intensity of the usual highest emission transition $^2F_{5/2}$ (5) → $^2F_{7/2}$ (3) of Yb^{3+} ions at around 1030 nm which is used as laser output in Yb^{3+}-doped laser materials, is probably due to the direct excitation of the foot of the 968 nm absorption line of the garnet structure due to the overlapping of the two 0-phonon absorption lines.

The absence of Yb^{3+} aggregates from TEM-EDX measurements both in grains and in grain boundaries excludes the classical explanation of the quenching of $Yb^{3+2}F_{5/2}$ (5) excited level by resonant migration of $^2F_{7/2}$ (1) ← →$^2F_{5/2}$ (5). Consequently this is another evidence of the role played by the distorted sites on the surface leading directly to nonradiative dissipation of the energy in the surroundings. These nonradiative transitions are favored by the observation in TEM of an amorphous phase associated with some grain boundaries.

Consequently, the high degree of perturbation at the surface of the grains might explain the presence of the 0-phonon line observed at around 975 nm only in absorption without any radiative de-excitation.

Identification of Yb^{3+} Pairs from the Cooperative Luminescence. Since the first observation by Nakazawa and Shionoya in $YbPO_4$,[55] cooperative luminescence of ytterbium ions has been reported in several hosts, crystals or glasses.[54,56] Cooperative luminescence is an effective way to indicate the formation of Yb^{3+} pairs and clusters in crystals and glasses. The cooperative emission center is assigned first to Yb^{3+} neighboring ions isolated in the host. The cooperative luminescence results from the simultaneous de-excitation of two Yb^{3+} ions in the blue range at around 500 nm which corresponds to the twice energy of the IR emission spectrum of the Yb^{3+} isolated ions.[55] Yb^{3+} ion is an unique case among rare earth ions allowing the observation of pairs due to the simplicity of the energy level diagram in the near IR and the absence of any Yb^{3+} isolated ion levels in the visible range.

The theoretical cooperative emission spectrum can be calculated taking into account all energetic combinations between Stark levels of the $^2F_{5/2}$ and $^2F_{7/2}$ manifolds. The cooperative luminescence spectrum $F(E)$ is then related to the infrared one $f(E)$ by

$$F(E) = \int f(E) f(E - E')\, dE' \quad (3)$$

The efficiency of the cooperative fluorescence is very low and naturally is favored for the shortest distances between Yb^{3+} ions. The calculation of the shortest distance d between Yb^{3+} ions in the dipole−dipole interaction has been estimated at d=4.5 Å.[57] In this YAG garnet crystallite grains, as the shortest distances is 3.67 Å between Yb^{3+} neighbors in substitution of Y^{3+} sites, an easy observation of Yb^{3+} ion pairs should occur. We have already pointed out these Yb^{3+} pairs in YAG bulky

dx.doi.org/10.1021/jp502882j | J. Phys. Chem. C XXXX, XXX, XXX−XXX

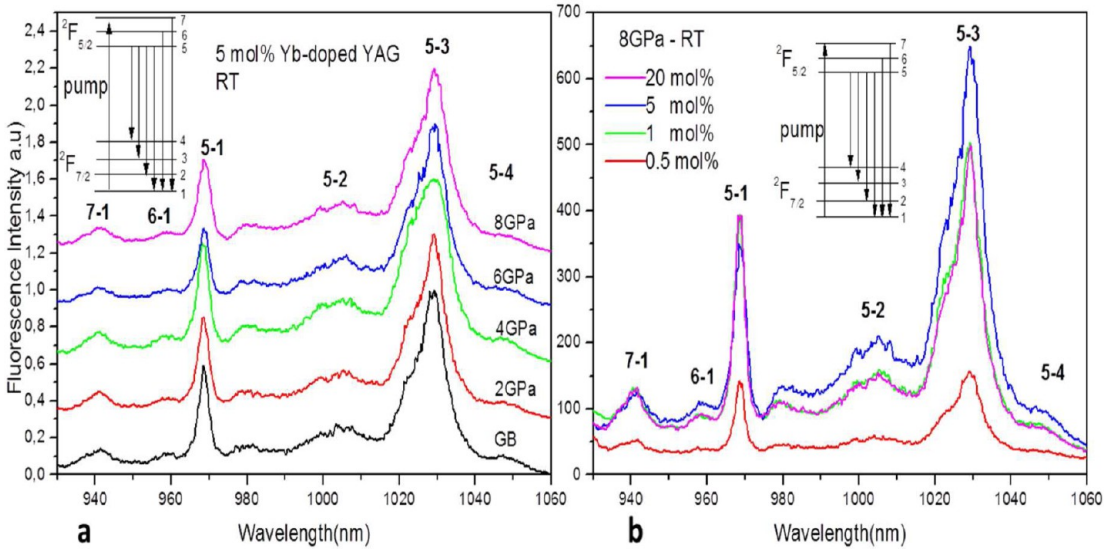

Figure 15. (a) Pressure dependence of the 5 mol % Yb^{3+}-doped YAG nanoceramics emission spectra at RT. (b) Concentration dependence of the x mol % Yb^{3+}-doped YAG nanoceramics emission spectra at RT under 8 GPa. Excitation into the level 7 by 917 nm of a Ti-sapphire laser.

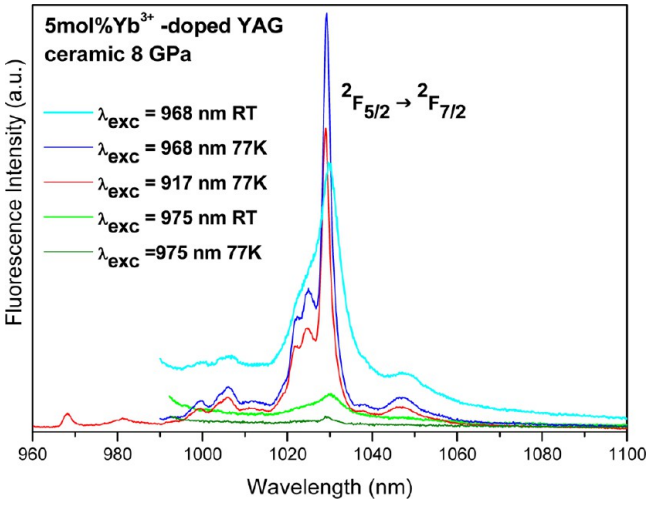

Figure 16. Selective laser excitation of the two 0-phonon lines of 5 mol % Yb^{3+}-doped YAG under 8 GPa at RT and 77 K.

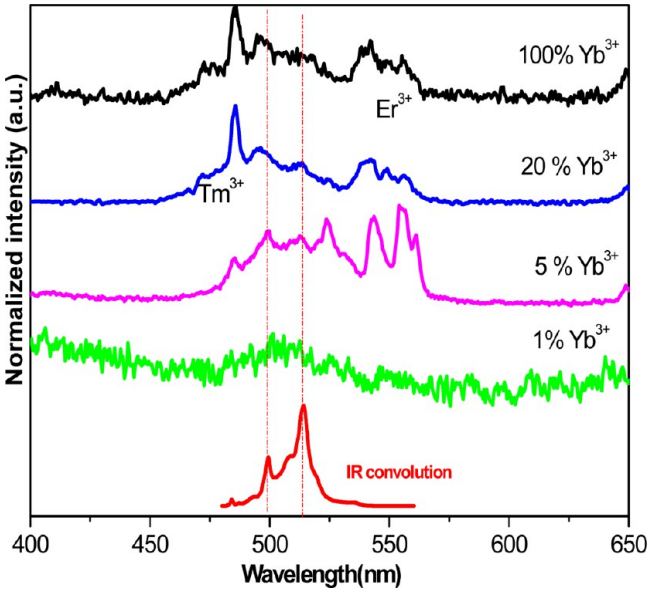

Figure 17. Cooperative luminescence of Yb^{3+} pairs in *x* mol % Yb^{3+}-doped YAG nanoceramics in the visible range (*x* = 1, 5, 20, and 100).

crystals above 5 mol % Yb^{3+}[32] and even more easily in YAG nanocrystals of smaller volume above 1 mol % Yb^{3+}.[35] Under pumping into the 0-phonon line in the near IR with an OPO pulsed laser at 968 nm, we observe a bluish-green light for Yb^{3+}-doped YAG nanoceramics as shown by the normalized spectra in Figure 17. Obviously, the population of Yb^{3+} pairs depends on the introduced Yb^{3+} ions. The convolution spectrum drawn fits well the experimental spectrum of the cooperative luminescence and moreover allows clearly for the separation between Yb^{3+} pairs and Tm^{3+}- Er^{3+} rare earth impurities from the raw materials. The time-resolved spectroscopy of the cooperative luminescence spectra is really a good probe of the presence of both pairs and impurities on the basis of the short lifetime of pairs and the higher lifetimes of Tm^{3+} and Er^{3+} ions as we have already shown it earlier.[32] In all Yb^{3+}-doped materials, Tm^{3+} and Er^{3+} impurities observed by up-conversion energy transfer process between Yb^{3+} sensitizer ions and either Tm^{3+} or Er^{3+} activator ions, contribute to the quenching of Yb^{3+} ions in glasses[54,56] and in crystals.[32,35,50,57] In this example we can say the materials are relatively clean since the Tm^{3+} or Er^{3+} ions intensity of the up-converted emission spectrum is very weak with respect of other garnet crystals examined by us.

In conclusion, Yb^{3+} ion pairs observed in the Yb^{3+}-doped YAG nanoceramics belong only to the grains of YAG garnet structure containing radiative Yb^{3+} isolated centers and not to the surface of the grains which play the role of the grain boundaries since we have shown that Yb^{3+} distorted sites of the surface do not give rise to any radiative transition. It also means the quenching of these Yb^{3+} isolated distorted ions cannot come from Yb^{3+} aggregates at the surface, which is in agreement with the absence of Yb^{3+} segregation phenomenon in these samples contrary to Ce^{3+} and Nd^{3+} ions.

Decays of the $Yb^{3+}{}^2F_{5/2}$ (5) Excited Level. The decay profiles of the $^2F_{5/2}$ (5) excited level, monitored at 1030 nm and associated with the 0-phonon line, shown in Figures 18), have almost an exponential profile for 5 mol % Yb^{3+}-doped nanoceramics independently of the sintering pressure. Figure

dx.doi.org/10.1021/jp502882j | J. Phys. Chem. C XXXX, XXX, XXX−XXX

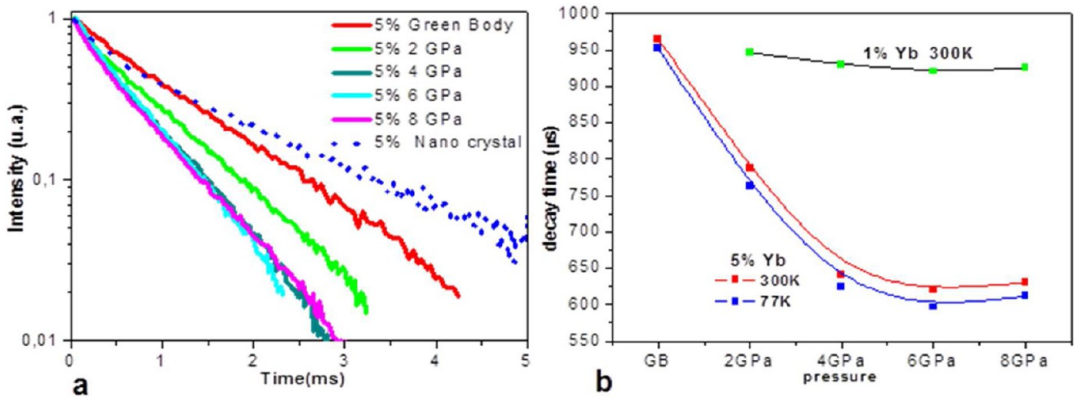

Figure 18. (a) Pressure dependence of the $^2F_{5/2}$ (5) decay profiles of 5 mol % Yb^{3+}-doped nanoceramics at RT (green body, 2, 4, 6, and 8 GPa respectively and nanocrystal in dots); (b) pressure dependence of the $^2F_{5/2}$ (5) level decay times in both 1 and 5 mol % Yb^{3+}-doped nanoceramics at RT and 77 K.

18) displays the notable decrease of the decay times when the sintering pressure is increasing. This quenching phenomenon means there is an increase of the nonradiative links due to the increasing of the pressure that is to say the increasing of perturbation on Yb^{3+} sites with a stronger effect on the sites in the vicinity of the grain boundaries.

The decay time of 1 mol % Yb^{3+}-doped nanoceramics is constant at RT due to the absence of interaction by resonance between Yb^{3+} ions since the average distances between Yb^{3+} sites are too high to create radiative energy transfer. This is also confirmed by the very small signal in Figure 17 of the cooperative luminescence associated with Yb^{3+} pairs in 1 mol % Yb^{3+} and the absence of any energy transfer to Er^{3+} and Tm^{3+} impurities.

Comparison between Nano and Microceramics. Such analysis of the structural and optical properties of Yb^{3+}-doped nanoceramics can be used with those of Nd^{3+}-doped nanoceramics for comparison with microceramics. Generally, the efficiency of luminescent nanocrystals is lower than their microsized counterparts due to surface defects. The nanocrystalline spinel ceramics of 28 nm are shown to exhibit a 50% increase in hardness over a corresponding order of magnitude reduction in grain size without a decline in density or fracture resistance. Additionally, the produced nanocrystalline ceramics have an optical transparency near theoretical.[58]

However, some specific advantages of transparent nanoceramics materials exist. First of all, nanoceramics can be of noncubic structure whereas microceramics should be of cubic structure so that the type of material compositions is largely increased. Several examples can be related as transparent sintered corundum with high macrohardness (HV10 = 20−21 GPa) and four-point bending strength (600−700 MPa; 750−900 MPa in three-point bending) are associated with a real in-line transmission of 55%−65% through polished plates.[59] Transmission physics and consequences for materials selection, manufacturing and applications can be seen in.[60] Fabrication of transparent LaAlO3/t-ZrO2 nanoceramics through controlled amorphous crystallization with an average grain size of 40 nm has been recently published.[61] Due to the nanoscale microstructure, the composite shows a transparency up to 55% at 800 nm (1 mm thick), Vickers hardness of 19.05 GPa, and fracture toughness of 2.64 MPam 1/2, respectively. It is expected to be a promising candidate for window materials. Single and polycrystalline transparent ceramic armor with different crystal structure have also been analyzed.[62]

On the contrary of microsized ones, two different types of nanoceramics materials can be mixed and consolidated. Let us mention, for example, nanoceramics materials doped with different ions or containing both linear and nonlinear optical materials into one bifunctional material with properties originate from individual grains.

Based on review of G. Liu and X. Chen,[63] nanoscale size of optical particles has significant effects on the excited state dynamics including radiative and nonradiative lifetimes, energy transfer, and thermalization phenomena. Many of these effects can be interpreted as consequences of modified ion-phonon interactions. Our results on the luminescence properties of Nd^{3+}:YAG nanoceramics are in favor of substantial differences to those reported for the respective single crystalline:[64] the emission line widths of $^4F_{3/2} \rightarrow {}^4I_{9/2}$ transitions are broader and increase as a function of sintering pressure. A specific feature of luminescence of Nd^{3+}:YAG nanoceramics is the appearance of hot emission transitions which originate most probably from enhanced thermalization of higher located terms from the $^4F_{3/2}$ excited state. This is mainly due the lowest thermal conductivity of nanoceramics compared to YAG crystal and polycrystalline ceramics composed of microsize grains.[65] Nanoceramics materials show a glass-like behavior.

This short review is in favor of advanced research of promising nanoceramics materials.

CONCLUSIONS

Our approach in the structural analysis of Yb^{3+}-doped YAG nanoceramics samples by conjugation of both TEM-EDX and optical techniques was shown. Yb^{3+}-doped YAG nanopowders were prepared using modified Pechini method with the objective to fabricate nanoceramics composed of nanosized grains by the low temperature-high pressure sintering technique (LTHP) which is a relatively simple method to be developed. The samples were sintered at temperature 450 °C during 1 min to avoid YAP phase formation and pressurized between 2 and 8 GPa. The sample pressurized at 8 GPa is characterized by the highest transparency and XRD confirms the $Y_3Al_5O_{12}$ garnet structure of the grains of ∼21 nm average size.

Yb^{3+} ion distribution has been analyzed by both spectroscopy of Yb^{3+} pairs from the co-operative luminescence phenomenon and TEM-EDX evaluation in grains and grain boundaries. EDX analysis at the TEM scale provides unambiguous results on a clear tendency of almost uniform Yb^{3+} distribution between grains and grain boundaries in nanoceramics like in bulky

dx.doi.org/10.1021/jp502882j | J. Phys. Chem. C XXXX, XXX, XXX−XXX

ceramics and in contrary with Ce^{3+} and Nd^{3+} activator results. Yb^{3+} ion pairs, with small population, observed by co-operative luminescence belong only to the Yb^{3+}-doped YAG nanograins of garnet structure containing radiative Yb^{3+} isolated centers and not to the surface of the grains which play the role of the grain boundaries since we have shown that Yb^{3+} distorted sites of the surface do not give rise to any radiative transition.

An important new observation has been made with the absorption line $^2F_{7/2}$ (1) → $^2F_{5/2}$ (5) at 975.7 nm at 4 K and room temperature, in addition of the 0-phonon line of the YAG structure of grains at 968 nm similar to that of bulky YAG single crystals. We have discussed the question concerning the origin of this new 0-phonon line relaxing only by nonradiative transitions and conclude that this line might be assigned rather to Yb^{3+} distorted sites on the grain surfaces of YAG nanoceramics in contact with an amorphous phase, with possibly additional traces of Yb^{3+}-doped α-Al_2O_3 single crystals of too weak population not enough to be detected either by XRD or by TEM. The evidence of the distorted sites at the surface leading directly to nonradiative dissipation of energy in the surroundings is in agreement with the TEM observation of a few amorphous phases in grain boundaries.

Rare earth-doped nanoceramics shows a glass-like behavior and need to be improved to be applied as optical materials. As an example the efficiency of luminescent nanocrystals is lower than their microsized counterparts due to quencher surface defects which need to be characterized. The absence of Yb^{3+} aggregates with high concentration from TEM-EDX measurements in both grains and grain boundaries excludes the explanation of the pressure quenching of $Yb^{3+2}F_{5/2}$ (5) excited level by resonant migration of $^2F_{7/2}$ (1) ← →$^2F_{5/2}$ (5). This quenching should be rather associated with an increase of the nonradiative links due to increasing of the pressure during sintering on Yb^{3+} sites with a stronger effect in the vicinity of the grain boundaries.

At this point of our knowledge on rare earth-doped nanoceramics, some physical limitations lead to the conclusion we cannot propose nanoceramics as a suitable material for laser or even scintillating applications, but might be interesting as a cheap technology for LED ceramics phosphors, windows and increased hardness.

Netherveless, nanoceramics worthwhile to be developed since this is possible to obtain a large variety of nanoceramics transparent materials of noncubic structure whereas they should be specifically of cubic structure with microceramics.

AUTHOR INFORMATION

Corresponding Author

*Tel.: +33 472 44 82 71. E-mail: georges.boulon@univ-lyon1.fr.

Notes

The authors declare no competing financial interest.

ACKNOWLEDGMENTS

The research exchange program between the Polish Academy of Sciences (PAS) and CNRS (France) is acknowledged. Thanks are due to the Department of Chemistry of the University of Wroclaw for the access of low temperature absorption measurements and to the CLYM (Centre Lyonnais de Microscopie- http://clym.insa-lyon.fr) for the access to the JEOL 2010F 200 kV microscope. The work was supported by Wroclaw Research Centre EIT+ within the project "The Application of Nanotechnology in Advanced Materials" - NanoMat (POIG.01.01.02-02-002/08) cofinanced by the European Regional Development Fund (Operational Programme Innovative Economy, 1.1.2).

REFERENCES

(1) Geusic, J. E.; Marcos, H. M.; Van Uitert, L. G. Laser Oscillations in Nd-doped Yttrium Aluminum, Yttrium Gallium and Gadolinium Garnets. *Appl. Phys. Lett.* **1964**, *4*, 182−184.

(2) Ikesue, A. Polycrystalline Nd:YAG Ceramics Lasers. *Opt. Mater.* **2000**, *19*, 183−187.

(3) Wang, H. M.; Simmonds, M. C.; Huang, Y. Z.; Rodenburg, J. M. Synthesis of Nanosize Powders and Thin Films of Yb-doped YAG by Sol-Gel Methods. *Chem. Mater.* **2003**, *15*, 3474−3480.

(4) Ikesue, A.; Kinoshita, T.; Kamata, K.; Yoshida, K. Fabrication and Optical Properties of High-Performance Polycrystalline Nd:YAG Ceramics For Solid-State Lasers. *J. Am. Ceram. Soc.* **1995**, *78*, 1033.

(5) Ikesue, A.; Furusato, I.; Kamata, K. Fabrication of Polycrystalline, Transparent YAG Ceramics by a Solid-State Reaction Method. *J. Am. Ceram. Soc.* **1995**, *78*, 225−228.

(6) Ikesue, A.; Aung, Y. L.; Yoda, T.; Nakayama, S.; Kamimura, T. Fabrication and Laser Performance of Polycrystal and Single Crystal Nd:YAG by Advanced Ceramic Processing. *Opt. Mater.* **2007**, *29*, 1289−1294.

(7) Shoji, I.; Taira, T.; Ikesue, A. Thermally-Induced-Birefringence Effects of Highly Nd^{3+}-doped $Y_3Al_5O_{12}$ Ceramic Lasers. *Opt. Mater.* **2007**, *29*, 1271−1276.

(8) Lu, J.; Prabhu, M.; Xu, J.; Ueda, K.; Yagi, H.; Yanagitani, T.; Kaminskii, A. A. High Efficiency 2% Nd:YAG Ceramic Laser. *Appl. Phys. Lett.* **2000**, *77*, 3707−3709.

(9) Lu, J.; Song, J.; Prabhu, M.; Xu, J.; Ueda, K.; Yagi, H.; Yanagitani, T.; Kudryasshov, A. High-Power Nd: $Y_3Al_5O_{12}$ Ceramic Laser. *Jpn. J. Appl. Phys. Part 2* **2000**, *39*, L1048−L1050.

(10) Lu, J.; Prabhu, M.; Song, J.; Li, C.; Xu, J.; Ueda, K.; Yagi, H.; Yanagitani, T.; Kaminskii, A. Highly Efficient Nd: $Y_3Al_5O_{12}$ Ceramic Laser. *Jpn. J. Appl. Phys., Part 2* **2001**, *40*, L552−L554.

(11) Yagi, H.; Yanagitani, T.; Yoshida, H.; Nakatsuka, M.; Ueda, K. The Optical Properties and Laser Characteristics of Cr^{3+} and Nd^{3+} Co-doped $Y_3Al_5O_{12}$ Ceramics. *Opt. Laser Technol.* **2007**, *39*, 1295−1300.

(12) Hreniak, D.; Gierlotka, S.; Łojkowski, W.; Stręk, W.; Mazur, P.; Fedyk, R. High-Pressure Induced Structural Decomposition of RE-doped YAG Nanoceramics. *Solid State Phenom.* **2005**, *106*, 17−22.

(13) Fedyk, R.; Hreniak, D.; Łojkowski, W.; Strek, W.; Matysiak, H.; Grzanka, E.; Gierlotka, S.; Mazur, P. Method of Preparation and Structural Properties of Transparent YAG Nanoceramics. *Opt. Mater.* **2007**, *29*, 1252−1257.

(14) Goldburt, E. T.; Kulkarni, B.; Bharagava, R. N.; Tylor, J.; Libera, M. Size Dependent Efficiency in Tb Doped Y_2O_3 Nanocrystalline Phosphor. *J. Lumin.* **1997**, *72−74*, 190−192.

(15) Pechini, M. P., Method of Preparing Lead And Alkaline Earth Titanates and Niobates and Coating Method Using the Same to Form a Capacitor, 1967, US Patent 3,330,697.

(16) Liu, Y.; Zhan, J.; Ren, M.; Tang, K.; Yu, W.; Qian, Y. Hydrothermal Synthesis of Square Thin Flake CdS by Using Surfactants and Thiocarbohydrate. *Mater. Res. Bull.* **2001**, *36*, 1231−1236.

(17) Sun, L.; Yao, J.; Liu, C.; Liao, C.; Yan, C. Rare Earth Activated Nanosized Oxide Phosphors: Synthesis and Optical Properties. *J. Lumin.* **2000**, *87−89*, 447−450.

(18) Gallagher, D.; Bhargava, R.; Racz, J. Method of Manufacturing Encapsulated Doped Particles. 1996, US Patent 5,525,377.

(19) Bowen, P.; Carry, C. From Powders to Sintered Pieces: Forming, Transformations and Sintering of Nanostructured Ceramic Oxides. *Powder Technol.* **2002**, *128*, 248−255.

(20) Kear, B. H.; Colaizzi, J.; Mayo, W. E.; Liao, S. C. On the Processing of Nanocrystalline and Nanocomposite Ceramics. *Scripta Mater.* **2001**, *44*, 2065−2068.

(21) Liao, S. C.; Pae, K. D.; Mayo, W. E. Theory of High Pressure/Low Temperature Sintering of Bulk Nanocrystalline TiO_2. *Acta Mater.* **1997**, *45*, 4027−4040.
(22) Rosenflanz, A.; Frey, M.; Endres, B.; Anderson, T.; Richards, E.; Schardt, C. Bulk Glasses and Ultrahard Nanoceramics Based on Alumina and Rare-Earth Oxides. *Nature* **2004**, *430*, 761−764.
(23) Xie, Z.; Yang, J.; Huang, X.; Huang, Y. Microwave Processing and Properties of Ceramics with Different Dielectric Loss. *J. Eur. Ceram. Soc.* **1999**, *19*, 381−387.
(24) Panneerselvam, M.; Subanna, G. N.; Rao, K. J. Translucent Yttrium Aluminum Garnet: Microwave-Assisted Route to Synthesis and Processing. *J. Mater. Res.* **2001**, *16*, 2273−2776.
(25) Hokamoto, K.; Tanaka, S.; Fujita, M.; Itoh, S.; Meyers, M. A.; Chen, H. C. High Temperature Shock Consolidation of Hard Ceramic Powders. *Physica B* **1997**, *239*, 1−5.
(26) Kaszuwara, W.; Leonowicz, M.; Januszewski, D.; Mendoza, G.; Davies, H. A.; Paszula, J. Consolidation of Magnetic Powders by Shock Compression. *J. Mater. Sci. Mater. Electron.* **1998**, *9*, 17−23.
(27) Groza, J. R. Nanosintering. *Nanostruct. Mater.* **1999**, *12*, 987−992.
(28) Groza, J. R.; Zavaliangos, A. Nanostructured Bulk Solids by Field Activated Sintering. *Rev. Adv. Mater. Sci.* **2003**, *5*, 24−33.
(29) Liao, S. C.; Chen, Y. J.; Kear, B. H.; Mayo, W. E. High Pressure/Low Temperature Sintering of Nanocrystalline Alumina. *Nanostruct. Mater.* **1998**, *10*, 1063−1079.
(30) Liao, S. C.; Pae, K. D.; Mayo, W. E. High Pressure and Low Temperature Sintering of Bulk Nanocrystalline TiO_2. *Mater. Sci. Eng., A* **1995**, *204*, 152−159.
(31) Choudhury, S.; Gandhi, A. S.; Jayaram, V. Bulk, Dense, Nanocrystalline Yttrium Aluminum Garnet by Consolidation of Amorphous Powders at Low Temperatures and High Pressures. *J. Am. Ceram. Soc.* **2003**, *86*, 247.
(32) Boulon, G. Why So Deep Research on Yb^{3+}-doped Optical Inorganic Materials? *J. Alloys. Compd.* **2008**, *451*, 1−11.
(33) Boulon, G.; Guyot, Y.; Yoshikawa, A. Optimization of the Gain in Yb3+-doped Cubic Laser Crystals of 99.99% Purity. *J. Rare Earths* **2009**, *27*, 616−618.
(34) Yoshikawa, A.; Boulon, G.; Laversenne, L.; Canibano, H.; Lebbou, K.; Collombet, A.; Guyot, Y.; Fukuda, T. Growth and Spectroscopic Analysis of Yb^{3+}-doped $Y_3Al_5O_{12}$ Fiber Single Crystals. *J. Appl. Phys.* **2003**, *94*, 5479−5488.
(35) Amami, J.; Hreniak, D.; Guyot, Y.; Zhao, W.; Boulon, G. Size-Effect on Concentration Quenching in Yb^{3+}-doped $Y_3Al_5O_{12}$ Nano-Crystals. *J. Lumin.* **2010**, *130*, 603−610.
(36) Esposito, L.; Serantoni, M.; Piancastelli, A.; Epicier, T.; Alderighi, D.; Pirri, A.; Toci, G.; Vannini, M.; Anghel, S.; Boulon, G. Integrated Analysis of Non-Linear Loss Mechanisms in Yb: YAG Ceramics for Laser Applications. *J. Europ. Cer. Soc.* **2012**, *32*, 2273−2281.
(37) Epicier, T.; Boulon, G.; Zhao, W.; Guzik, M.; Jiang, B.; Ikesue, A.; Esposito, L. Spatial Distribution of the Yb^{3+} Rare Earth Ions in $Y_3Al_5O_{12}$ And Y_2O_3 Optical Ceramics as Analyzed by TEM. *J. Mater. Chem.* **2012**, *22*, 18221−18229.
(38) Zhao, W.; Hreniak, D.; Boulon, G.; Strek, W.; Brenier, A.; Yin, M.; Gluchowski, P.; Lukowiak, A.; Wiglusz, R.; Epicier, T. Spectroscopic Properties of Yb^{3+}-doped $Y_3Al_5O_{12}$ Nano-Ceramics Obtained Under Different Sintering Pressures. *Radiat. Meas.* **2010**, *45*, 304−306.
(39) Strek, W.; Marciniak, L.; Gluchowski, P.; Hreniak, D. Infrared Laser Stimulated Broadband White Emission of Yb^{3+}:YAG Nano-ceramics. *Opt. Mater.* **2013**, *35*, 2013−2017.
(40) Zhao, W.; Mancini, C.; Amans, D.; Boulon, G.; Epicier, T.; Min, Y.; Yagi, H.; Yanagitani, T.; Yanagida, T.; Yoshikawa, A. Evidence of the Inhomogeneous Ce^{3+} Distribution Across Grain Boundaries in Transparent Polycrystalline Ce^{3+}-doped $(Gd,Y)_3Al_5O_{12}$ Garnet Optical Ceramics. *Jpn. J. of Appl. Phys.* **2010**, *49*, 022602.
(41) Zhao, W.; Anghel, S.; Mancini, C.; Amans, D.; Boulon, G.; Epicier, T.; Shi, Y.; Feng, X. Q.; Pan, Y. B.; Chani, V.; Yoshikawa, A. Ce^{3+} Dopant Segregation in $Y_3Al_5O_{12}$ Optical Ceramics. *Opt. Mater.* **2011**, *33*, 684−687.
(42) Zhydachevskii, Y.; Syvorotka, I. I.; Vasylechko, L.; Sugak, D.; Borshchyshyn, I. D.; Luchechko, A. P.; Vakhula, Ya.I.; Ubizskii, S. B.; Vakiv, M. M.; Suchocki, A. Crystal Structure and Luminescent Properties of Nanocrystalline YAG and YAG:Nd Synthesized by Sol-Gel Method. *Opt. Mater.* **2012**, *34*, 1984−1989.
(43) Ramirez, M. O.; Wisdom, J.; Li, H.; Aung, Y. L.; Stitt, J.; Messing, G. L.; Dierolf, V.; Liu, Z.; Ikesue, A.; Byer, R. L.; Gopalan, V. Three-Dimensional Grain Boundary Spectroscopy in Transparent High Power Ceramic Laser Materials. *Opt. Express* **2008**, *16*, 5965.
(44) Xu, X.; Zhao, Z.; Song, P.; Zhou, G.; Xu, J.; Deng, P. Structural, Thermal, and Luminescent Properties of Yb-doped $Y_3Al_5O_{12}$ Crystals. *J. Opt. Soc. Am. B* **2004**, *21*, 543−547.
(45) Chani, V. I.; Yoshikawa, A.; Kuwano, Y.; Hasegawa, K.; Fukuda, T. Growth of $Y_3Al_5O_{12}$:Nd Fiber Crystals by Micro-Pulling-Down Technique. *J. Cryst. Growth* **1999**, *204*, 155−162.
(46) Chani, V. I. Iron Garnet Films For Optical Isolators In Wavelength Range 800−1300 nm, in Thin Films in Optics, *Proc. SPIE 1125*; Tschudi, T. T., Ed.; SPIE: Bellingham, WA, 1990; p 107.
(47) Chani, V. I. *Fiber Crystal Growth from the Melt*; Fukuda, T., Rudolph, P., Uda, S., Eds.; Springer−Verlag: Berlin, 2004; p 129.
(48) Simura, R.; Yoshikawa, A.; Uda, S. The Radial Distribution of Dopant (Cr, Nd, Yb, or Ce) in Yttrium Aluminum Garnet (Y3Al5O12) Single Crystals Grown by the Micro-Pulling-Down Method. *J. Cryst. Growth* **2009**, *311*, 4763−4769.
(49) Jiang, B.; Gong, Zh.; Chen, M.; Li, J.; Liu, W.; Pan, Y. Comparative Spectroscopic Investigation of $Yb_{3x}Y_{3(1-X)}Al_5O_{12}$ (X = 3, 5, 10 and 15%) Transparent Ceramics. *Bull. Russ. Acad. Sci., Phys.* **2012**, *76*, 643−647.
(50) Boulon, G.; Guyot, Y.; Canibano, H.; Hraiech, S.; Yoshikawa, A. Characterization and Comparison of Yb^{3+}-doped $YA1O_3$ Perovskite Crystals (Yb:YAP) with Yb^{3+}-doped $Y_3Al_5O_{12}$ Garnet Crystals (Yb:YAG) For Laser Application. *J. Opt. Soc. Am. JOSA B* **2008**, *25*, 884−896.
(51) Song, Q.; Li, C.-R.; Li, J.-Y.; Ding, W.-Y.; Li, S.-F.; Xu, J.; Deng, X.-L.; Song, C.-L. Photoluminescence Properties of the Yb:Er Co-doped Al_2O_3 Thin Film Fabricated by Microwave ECR Plasma Source Enhanced RF Magnetron Sputtering. *Opt. Mater.* **2006**, *28*, 1344−1349.
(52) Jusza, A.; Anders, K.; Jastrzebska, A.; Polis, P.; Olszyna, A.; Kus, M.; Kunicki, A.; Piramidowicz, R. Luminescent and Structural Properties of Yb^{3+}-doped Al_2O_3 Nanopowders. *Opt. Mater.* **2011**, *33*, 1487−1491.
(53) Krebs, J. K.; Happek, U. Yb^{3+} Energy Levels in α-Al_2O_3. *J. Lumin.* **2001**, *94*−*95*, 65−68.
(54) Guyot, Y.; Steimacher, A.; Belançon, M. P.; Medina, A. N.; Baesso, L.; Lima, S.; Andrade, L. H. C.; Brenier, A.; Jurdyc, A. M.; Boulon, G. Spectroscopic Properties, Concentration Quenching, and Laser Investigations of Yb^{3+}-Doped Calcium Aluminosilicate Glasses. *J. Opt. Soc. Am. JOSA B* **2011**, *28*, 2510−2517.
(55) Nakazawa, E.; Shionoya, S. Cooperative Luminescence in $YbPO_4$. *Phys. Rev. Lett.* **1970**, *25*, 1710−1712.
(56) Boulon, G. *Co-Operative Processes in Yb^{3+}-doped Materials in Frontiers Developments in Optics and Spectroscopy*, Di Bartolo, B., Forte, O.; Eds.; Book available free on http://www.bc.edu/schools, September 2007; Vol. *5*, pp 1−22.
(57) Auzel, F.; Goldner, P. Towards Rare-Earth Clustering Control in Doped Glasses. *Opt. Mater.* **2001**, *16*, 93−103.
(58) Wollmershauser, J. A.; Feigelson, B. N.; Gorzkowski, E. P.; Ellis, C. T.; Goswami, R.; Qadri, S. B.; Tischler, J. G.; Kub, F. J.; Everett, R. K. An Extended Hardness Limit in Bulk Nanoceramics. *Acta Mater.* **2014**, *69*, 9−16.
(59) Krell, A.; Blank, P.; Ma, H.; Hutzler, T.; Van Bruggen, M. P. B.; Apetz, R. Transparent Sintered Corundum with High Hardness and Strength. *J. Am. Ceram. Soc.* **2003**, *86*, 12−18.
(60) Krell, A.; Hutzler, T.; Klimke, J. Transmission Physics and Consequences for Materials Selection, Manufacturing, and Applications. *J. Eur. Ceram. Soc.* **2009**, *29*, 207−221.

(61) Mei, L.; He, G.; Wang, L.-L.; Liu, G.-H.; Li, J.-T. Fabrication of Transparent $LaAlO_3$/T-ZrO_2 Nanoceramics Through Controlled Amorphous Crystallization. *J. Eur. Ceram. Soc.* **2011**, *31*, 1603−1609.
(62) Krell, A.; Strassburger, E.; Hutzler, T.; Klimke, J. Single and Polycrystalline Transparent Ceramic Armor with Different Crystal Structure. *J. Am. Ceram. Soc.* **2013**, *96*, 2718−2721.
(63) Liu, G.; Chen, X. Spectroscopic Properties of Lanthanides in Nanomaterials, Chapter 233. *Handbook Phys. Chem. Rare Earths* **2007**, *37*, 99−169.
(64) Hreniak, D.; Fedyk, R.; Bednarkiewicz, A.; Strek, W.; Łojkowski, W. Luminescence Properties of Nd:YAG Nanoceramics Prepared by Low Temperature High Pressure Sintering Method. *Opt. Mater.* **2007**, *29*, 1244−1251.
(65) Mucha, J.; Chuchmała, A.; Hreniak, D.; Jezowski, A.; Strek, W. Heat Transfer in Transparent YAG Nanoceramic. *J. Ceram. Sci. Technol.* **2011**, *2*, 179−182.